

# SAnTex: A Python-based Library for Seismic Anisotropy Calculation

Utpal Singh <sup>1</sup>, Sinan Özaydın  <sup>1</sup>, Vasileios Chatzaras  <sup>1</sup>, and Patrice Rey<sup>1</sup>

<sup>1</sup> The University of Sydney, School of Geosciences, Sydney, NSW, Australia

DOI: [10.21105/joss.06886](https://doi.org/10.21105/joss.06886)

## Software

- [Review ↗](#)
- [Repository ↗](#)
- [Archive ↗](#)

---

Editor: [Rachel Kurchin](#) 

## Reviewers:

- [@elena-pascal](#)
- [@hakonanes](#)

Submitted: 30 April 2024

Published: 20 May 2025

## License

Authors of papers retain copyright and release the work under a Creative Commons Attribution 4.0 International License ([CC BY 4.0](#)).

## Summary

Seismic anisotropy, the directional dependency of seismic wave velocities, is important for mapping the Earth's structure and understanding geodynamic processes. Seismic anisotropy primarily stems from the development of mineral crystallographic preferred orientation (i.e. texture) during the plastic deformation of rocks. In-depth analysis of data from texture characterization techniques like Electron Backscatter Diffraction (EBSD) enables the determination of mineral and bulk-rock elastic properties. Although the influences of pressure, temperature, and melt on elastic properties and seismic anisotropy is well understood, they are often disregarded. To help address this gap, we developed SAnTex: Seismic Anisotropy from Texture, an open-source Python library that calculates the full elastic tensor of rocks from modal mineral composition, crystallographic orientation, and a crystal stiffness tensor catalogue that accounts for the dependency of elasticity with pressure, temperature and melt. The elastic wave velocities ( $V_p$ ,  $V_s$ ) and seismic anisotropy are calculated from the full elastic tensors. SAnTex extends its utility beyond the solidus by estimating melt volume in a rock and assessing its impact on seismic wave velocities and anisotropy.

## Statement of need

Understanding seismic wave velocities and anisotropy is crucial for deciphering the composition, structure, and rheological behaviour of the Earth's crust and mantle. Seismic anisotropy primarily emerges from the propagation of waves through rocks that have developed crystallographic preferred orientations (CPO) as a result of plastic deformation ([Mainprice & Nicolas, 1989](#)). The rock composition (e.g., mineralogy, presence of melt or water) and microstructure (e.g., grain size, microcracks) can further influence both seismic velocities and anisotropy ([Almqvist & Mainprice, 2017](#); [Karato et al., 2008](#); [Nicolas & Christensen, 1987](#)).

Seismic anisotropy calculations that rely on the integration of textural data obtained by Electron Backscatter Diffraction (EBSD) with experimentally determined elastic stiffness tensors have become standard practice in rock-based geodynamic studies ([Bernard et al., 2019](#); [Boneh et al., 2015](#); [Chatzaras & Kruckenberg, 2023](#); [Demouchy et al., 2019](#); [Jung et al., 2006](#); [Tommasi & Ishikawa, 2014](#); [Vauchez et al., 2005](#)). While established tools like MTEX ([Mainprice et al., 2015](#)) allow for robust texture analysis, they rely on 'reference stiffness tensors' derived under ambient conditions to constrain elastic properties (Fig. 1c). However, first-principles simulations and laboratory experiments reveal that reference stiffness tensors can significantly deviate from those at deep crustal and mantle conditions ([Kumazawa, 1969](#); [Kumazawa & Anderson, 1969](#); [Qian et al., 2017](#); [Su et al., 2021](#); [Walker, 2012](#)). Therefore, seismic properties derived from textural analyses need to integrate the effects of temperature, pressure, and melt.

Melt characteristics — such as fraction, shape, distribution, and orientation have well-understood effects on seismic properties ([Hammond & Humphreys, 2000](#); [Kendall, 1994](#);

Takei, 1998). However, the combined effect of melt and rock texture is less commonly considered (Holtzman & Kendall, 2010; Lee et al., 2017). Functionalities that allow us to estimate how the combination of texture-induced anisotropy and melt affect the elastic properties under varying pressure and temperature have yet to be incorporated into an open-source toolkit.

To address these gaps, we have developed SAnTex (Seismic Anisotropy from Texture), a free, open-source Python library. Built upon open-source libraries such as ORIX (Johnstone et al., 2020) for orientation analysis, SanTeX provides an accessible platform for the geoscientific community, embodying the principles of free and open science, and promoting reproducibility and transparency.

## Methods

Hooke's law characterizes the response of materials to tensile or compressive forces. In its generalized formulation, the law asserts that the stress tensor is linearly related to the strain tensor through the material's stiffness properties (Timoshenko & Goodier, 1969):

$$\sigma_{ij} = C_{ijkl}\epsilon_{kl} \quad (1)$$

where  $\sigma_{ij}$  and  $\epsilon_{kl}$  are the components of the stress and strain tensors, respectively, while  $C_{ijkl}$  is a 4th-order stiffness tensor with 81 elements representing elastic moduli. In this general form, Hooke's law can account for the anisotropy and directionality of the elastic properties of materials.

The stiffness tensors are derived from laboratory experiments, and represent the intrinsic elastic properties of individual minerals. The calculated effective stiffness tensors, on the other hand, provide a more realistic representation of rock behaviour in the Earth's crust and upper mantle. They account for the combined influence of pressure and temperature.

The pressure and temperature dependence of elastic constants is primarily linear but can include non-linear effects that can be approximated up to second-order terms using a Taylor series expansion (Faccenda et al., 2024; Frisillo & Barsch, 1972; Kumazawa, 1969; Mainprice & Silver, 1993).

$$C_{ijkl}(P, T) = C_{ijkl}(P_0, T_0) + \frac{\partial C_{ijkl}}{\partial P} \Big|_{(P_0, T_0)} \Delta P + \frac{\partial C_{ijkl}}{\partial T} \Big|_{(P_0, T_0)} \Delta T + \mathcal{O}(\Delta P^2, \Delta T^2) \quad (2)$$

Within SAnTex,  $C_{ijkl}(p, T)$  is the resultant or effective stiffness tensor,  $C_{ijkl}(P_0, T_0)$  is the reference stiffness tensor obtained at ambient conditions, with  $P_0 = 10^{-4}$ ~GPa and  $T_0 \approx 298$ ~K, and  $\Delta p$  and  $\Delta T$  are deviations from the ambient conditions. The partial derivatives  $\frac{\partial C_{ijkl}}{\partial p}$  and  $\frac{\partial C_{ijkl}}{\partial T}$  are obtained from the literature sources included in the data package within SAnTex.

Pressure and temperature have competing effects on the stiffness tensor. Higher temperatures increase atomic vibrations, making it easier for the material to deform, while higher pressures force atoms closer together, making it more difficult for the material to deform.

In the current version of SAnTex, melt is considered as a homogeneously distributed isotropic phase within an anisotropic host rock (Lee et al., 2017).

$$C_{ijkl}(P, T) = (1 - f_{\text{melt}}) \left( C_{ijkl}(P_0, T_0) + \frac{\partial C_{ijkl}}{\partial P} \Big|_{(P_0, T_0)} \Delta P + \frac{\partial C_{ijkl}}{\partial T} \Big|_{(P_0, T_0)} \Delta T + \mathcal{O}(\Delta P^2, \Delta T^2) \right) + f_{\text{melt}} \cdot C_{\text{melt}}(P, T) \quad (3)$$

The fraction of melt,  $f$ , can be controlled by the user.  $C_{melt}$  is the stiffness tensor of the melt, which assumes an anisotropic solid host rock and an evenly distributed isotropic melt (Lee et al., 2017). The approach currently incorporated in SAnTex overlooks the complex behaviour of melt, not including its viscosity, flow dynamics, and interaction with neighbouring minerals, which can influence the overall anisotropic properties of the system. Future updates of SAnTex will incorporate additional capabilities, such as modelling melt–grain interactions, to further refine the calculation of melt-induced anisotropy.

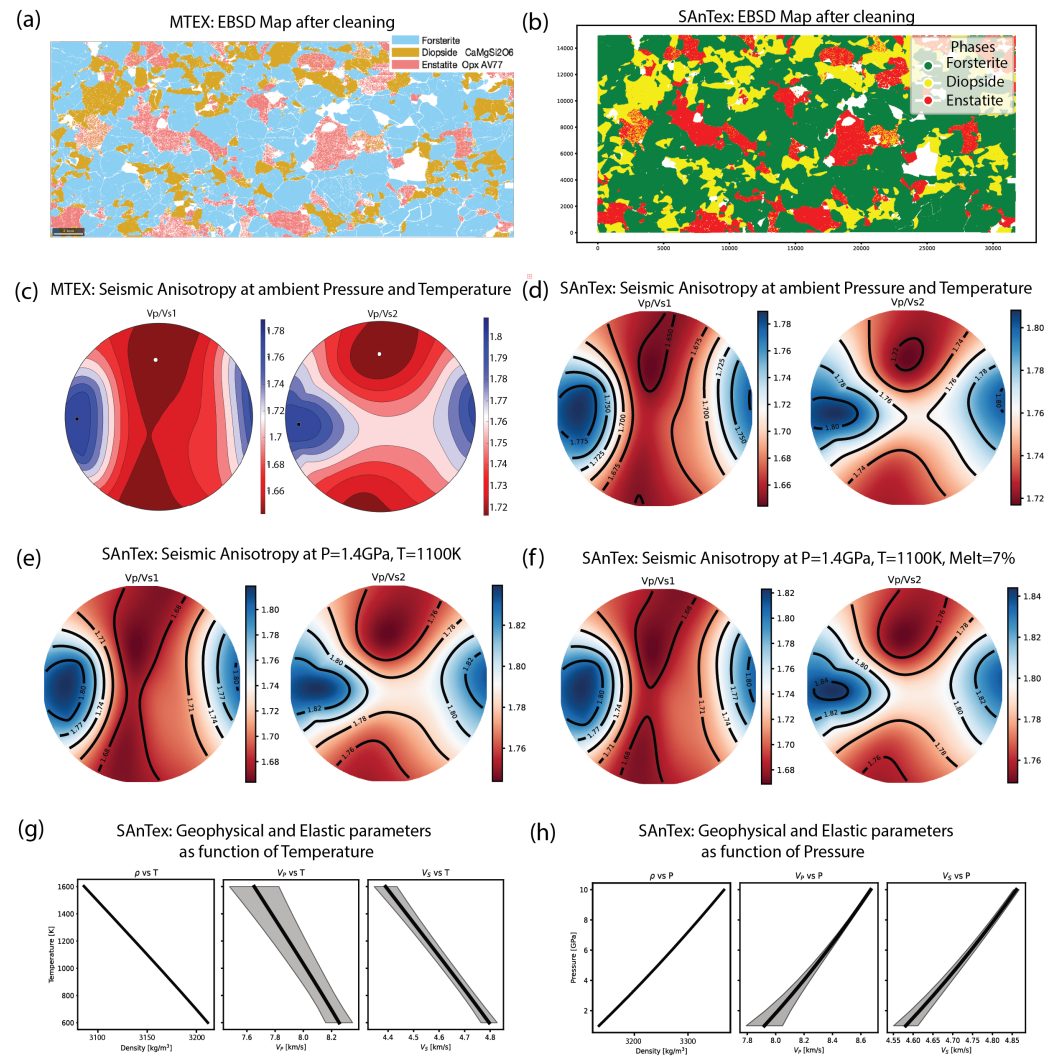


**Figure 1:** EBSD maps after cleaning using (a) MTEX and (b) SAnTex. Seismic Anisotropy maps using (c) MTEX at ambient pressure and temperature and SAnTex at (d) ambient pressure and temperature, (e) at 1.4 GPa and 1100° K, and (f) 1.4 GPa and 1100° K with 7% silicate melt. Density, P and S wave velocities against (g) temperature and (h) pressure. The gray shaded areas show the upper and lower Hashin-Shtrikman bounds scaled by a factor of 1000 to demonstrate the difference between lower and upper bounds.

SAnTex calculates seismic properties from EBSD crystal orientation data using the following steps:

1. Calculation of the effective tensor constants by incorporating pressure and temperature derivatives. SAnTex includes an inbuilt catalogue of minerals, for which it automatically calculates the stiffness tensors and density for a range of pressure and temperature

conditions.

2. Determination of the effective stiffness tensors by applying Taylor series expansion.
3. Computation of a mean stiffness tensor using the Voigt-Reuss-Hill bounds. These bounds provide an estimate for the effective elastic moduli of heterogeneous or anisotropic materials by averaging the Voigt (upper bound, corresponding to uniform strain) and Reuss (lower bound, corresponding to uniform stress) approximations.
4. Incorporation of the effect of melt on seismic properties through a nonlinear peridotite melting curve between solidus and liquidus (McKenzie & Bickle, 1988). Alternatively, a melt fraction value can be imposed by the user.

The capabilities of SAnTex are tested on previously published data using MTEX for a peridotite xenolith from Marie Byrd Land volcanic province in West Antarctica (Fig. 1) ([Chatzaras et al., 2016](#); [Chatzaras & Kruckenberg, 2023](#)). Here, we demonstrate that the outputs of SAnTex match those generated using MTEX, at ambient pressure and temperature conditions (Fig. 1c vs. 1d). Higher seismic anisotropies are calculated for the same sample, at equilibration temperature and pressure conditions corresponding to the lithospheric mantle (Fig. 1e). The effect of assumed 7% melt on seismic anisotropies calculated at the same equilibration conditions is shown in Fig. 1f. Fig. 1g and 1h shows seismic wave velocities and densities as a function of temperature and pressure for the same modal composition. The gray shaded areas show the upper and lower Hashin-Shtrikman bounds, which provide theoretical limits on the effective elastic properties of a composite material based on the volume fractions and properties of its constituent mineral phases.

## Package Summary

SAnTex allows for (Fig. 2):

1. Processing of EBSD data: Facilitates the processing and cleaning of EBSD data. It leverages the ORIX software package for the calculation of pole figures, pole density functions and inverse pole figures ([Johnstone et al., 2020](#)).
2. Tensor operations: Supports conversions between the Voigt matrix representation and full stiffness tensor forms. Additionally, tensor rotations are performed using orientations (Euler angles following the ZXZ convention) to transform tensors between different coordinate systems.
3. Material analysis: Includes a comprehensive mineral catalogue that facilitates the calculation of seismic properties based on a given mineralogical composition. Users may either select phases corresponding to EBSD-determined phase abundances or assume a modal mineral composition.
4. Calculation of seismic anisotropy: Computes seismic velocities and anisotropy across a range of pressure (0–13 GPa) and temperature (300–2000 K) conditions (Fig. 1d, e, f), and provides interactive 2D and 3D plots for visualizing the results (Fig. 3).
5. Calculation of isotropic velocities: Computes isotropic seismic wave velocities and Hashin-Shtrikman bounds ( $V_p$ ,  $V_s$ , and  $V_{bulk}$ ), along with the isothermal bulk modulus and density, under geological conditions ([Hacker & Abers, 2004](#)) (Fig. 1g, h). The calculated velocities and elastic properties can be fed to geophysical interpretation tools such as pide ([Ozaydin et al., 2025](#)).

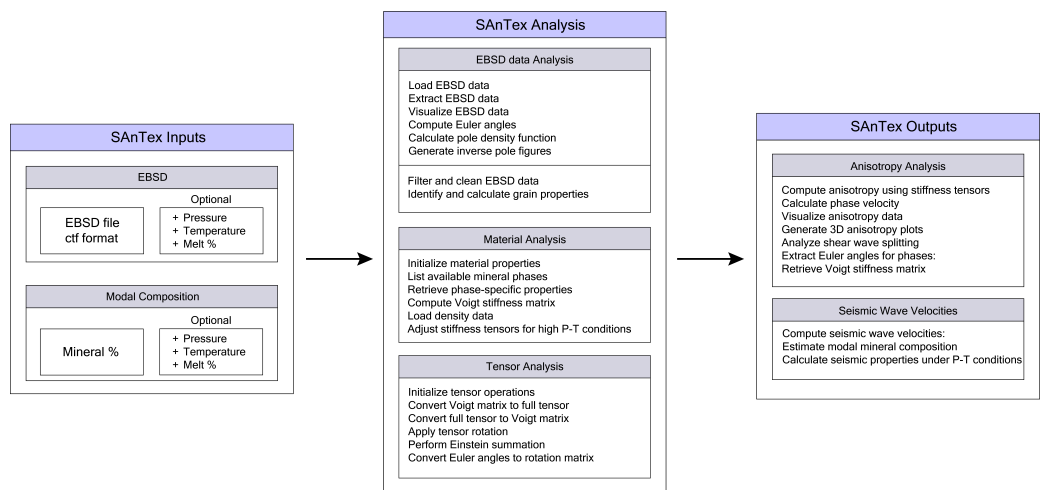


**Figure 2:** Workflow of SAnTex with fundamental methods and classes outlined.

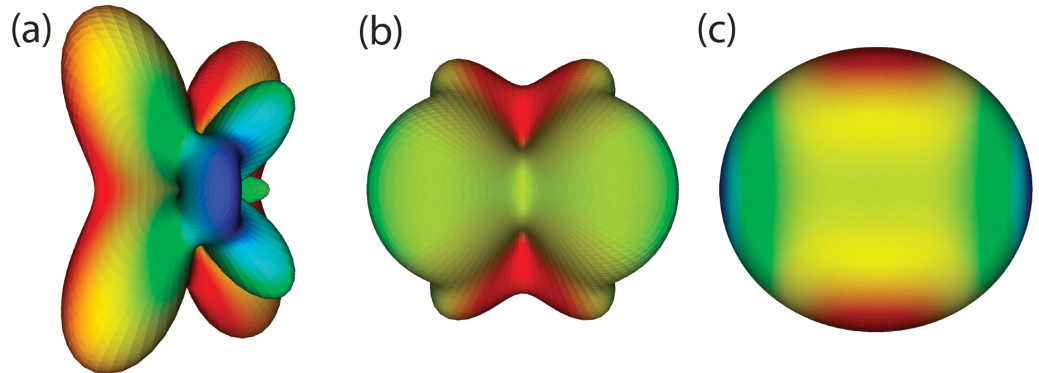


**Figure 3:** 3D visualisation of (a) Forsterite Vs splitting, (b) Olivine Vs splitting, (c) Olivine V<sub>p</sub>.

## Acknowledgements

This research was supported by the Australian Research Council grants ARC-DP220100709 and ARC-LP190100146. U. Singh acknowledges financial support from the School of Geosciences at The University of Sydney.

## References

- Almqvist, B. S. G., & Mainprice, D. (2017). Seismic properties and anisotropy of the continental crust: Predictions based on mineral texture and rock microstructure. *Reviews of Geophysics*, 55(2), 367–433. <https://doi.org/10.1002/2016RG000552>
- Bernard, R. E., Behr, W. M., Becker, T. W., & Young, D. J. (2019). Relationships Between Olivine CPO and Deformation Parameters in Naturally Deformed Rocks and Implications for Mantle Seismic Anisotropy. *Geochemistry, Geophysics, Geosystems*, 20(7), 3469–3494. <https://doi.org/10.1029/2019GC008289>
- Boneh, Y., Morales, L. F. G., Kaminski, E., & Skemer, P. (2015). Modeling olivine CPO evolution with complex deformation histories: Implications for the interpretation of seismic

- anisotropy in the mantle. *Geochemistry, Geophysics, Geosystems*, 16(10), 3436–3455. <https://doi.org/10.1002/2015GC005964>
- Chatzaras, V., & Kruckenberg, S. C. (2023). Effects of melt-percolation, refertilization and deformation on upper mantle seismic anisotropy: Constraints from peridotite xenoliths, Marie Byrd Land, West Antarctica. *Geological Society, London, Memoirs*, 56(1), 151–180. <https://doi.org/10.1144/M56-2020-16>
- Chatzaras, V., Kruckenberg, S. C., Cohen, S. M., Medaris Jr., L. G., Withers, A. C., & Bagley, B. (2016). Axial-type olivine crystallographic preferred orientations: The effect of strain geometry on mantle texture. *Journal of Geophysical Research: Solid Earth*, 121(7), 4895–4922. <https://doi.org/10.1002/2015JB012628>
- Demouchy, S., Tommasi, A., Ionov, D., Higgin, K., & Carlson, R. W. (2019). Microstructures, Water Contents, and Seismic Properties of the Mantle Lithosphere Beneath the Northern Limit of the Hangay Dome, Mongolia. *Geochemistry, Geophysics, Geosystems*, 20(1), 183–207. <https://doi.org/10.1029/2018GC007931>
- Faccenda, M., VanderBeek, B. P., Montserrat, A. de, Yang, J., Rappisi, F., & Ribe, N. (2024). ECOMAN: An open-source package for geodynamic and seismological modelling of mechanical anisotropy. *Solid Earth*, 15(10), 1241–1264. <https://doi.org/10.5194/se-15-1241-2024>
- Frisillo, A. L., & Barsch, G. R. (1972). Measurement of single-crystal elastic constants of bronzite as a function of pressure and temperature. *Journal of Geophysical Research (1896-1977)*, 77(32), 6360–6384. <https://doi.org/10.1029/JB077i032p06360>
- Hacker, B. R., & Abers, G. A. (2004). Subduction Factory 3: An Excel worksheet and macro for calculating the densities, seismic wave speeds, and H<sub>2</sub>O contents of minerals and rocks at pressure and temperature. *Geochemistry, Geophysics, Geosystems*, 5(1). <https://doi.org/10.1029/2003GC000614>
- Hammond, W. C., & Humphreys, E. D. (2000). Upper mantle seismic wave velocity: Effects of realistic partial melt geometries. *Journal of Geophysical Research: Solid Earth*, 105(B5), 10975–10986. <https://doi.org/10.1029/2000JB900041>
- Holtzman, B. K., & Kendall, J.-M. (2010). Organized melt, seismic anisotropy, and plate boundary lubrication. *Geochemistry, Geophysics, Geosystems*, 11(12). <https://doi.org/10.1029/2010GC003296>
- Johnstone, D. N., Martineau, B. H., Crout, P., Midgley, P. A., & Eggeman, A. S. (2020). Density-based clustering of crystal (mis)orientations and the orix Python library. *Journal of Applied Crystallography*, 53(5), 1293–1298. <https://doi.org/10.1107/S1600576720011103>
- Jung, H., Katayama, I., Jiang, Z., Hiraga, T., & Karato, S. (2006). Effect of water and stress on the lattice-preferred orientation of olivine. *Tectonophysics*, 421(1), 1–22. <https://doi.org/10.1016/j.tecto.2006.02.011>
- Karato, S., Jung, H., Katayama, I., & Skemer, P. (2008). Geodynamic Significance of Seismic Anisotropy of the Upper Mantle: New Insights from Laboratory Studies. *Annual Review of Earth and Planetary Sciences*, 36(1), 59–95. <https://doi.org/10.1146/annurev.earth.36.031207.124120>
- Kendall, J.-M. (1994). Teleseismic arrivals at a mid-ocean ridge: Effects of mantle melt and anisotropy. *Geophysical Research Letters*, 21(4), 301–304. <https://doi.org/10.1029/93GL02791>
- Kumazawa, M. (1969). The elastic constants of single-crystal orthopyroxene. *Journal of Geophysical Research*, 74(25), 5973–5980. <https://doi.org/10.1029/JB074i025p05973>
- Kumazawa, M., & Anderson, O. L. (1969). Elastic moduli, pressure derivatives, and temperature derivatives of single-crystal olivine and single-crystal forsterite. *Journal of Geophysical*

- Research (1896-1977), 74(25), 5961–5972. <https://doi.org/10.1029/JB074i025p05961>
- Lee, A. L., Walker, A. M., Lloyd, G. E., & Torvela, T. (2017). Modeling the impact of melt on seismic properties during mountain building. *Geochemistry, Geophysics, Geosystems*, 18(3), 1090–1110. <https://doi.org/10.1002/2016GC006705>
- Mainprice, D., Bachmann, F., Hielscher, R., & Schaeben, H. (2015). Descriptive tools for the analysis of texture projects with large datasets using MTEX: Strength, symmetry and components. *Geological Society, London, Special Publications*, 409(1), 251–271. <https://doi.org/10.1144/SP409.8>
- Mainprice, D., & Nicolas, A. (1989). Development of shape and lattice preferred orientations: Application to the seismic anisotropy of the lower crust. *Journal of Structural Geology*, 11(1), 175–189. [https://doi.org/10.1016/0191-8141\(89\)90042-4](https://doi.org/10.1016/0191-8141(89)90042-4)
- Mainprice, D., & Silver, P. G. (1993). Interpretation of SKS-waves using samples from the subcontinental lithosphere. *Physics of the Earth and Planetary Interiors*, 78(3-4), 257–280. [https://doi.org/10.1016/0031-9201\(93\)90160-B](https://doi.org/10.1016/0031-9201(93)90160-B)
- Nicolas, A., & Christensen, N. I. (1987). Formation of Anisotropy in Upper Mantle Peridotites - A Review. In *Composition, Structure and Dynamics of the Lithosphere-Asthenosphere System* (pp. 111–123). American Geophysical Union (AGU). <https://doi.org/10.1029/GD016p0111>
- Ozaydin, S., Li, L., Singh, U., Rey, P. F., & Manassero, M. C. (2025). Pide: Petrophysical Interpretation tools for geoDynamic Exploration. *Journal of Open Source Software*, 10(105), 7021. <https://doi.org/10.21105/joss.07021>
- Qian, W., Wang, W., Fan, Z., & Wu, Z. (2017). Elasticity of Orthoenstatite at High Pressure and Temperature: Implications for the Origin of Low  $V_p/V_p$  Zones in the Mantle Wedge. *Geophysical Research Letters*, 45. <https://doi.org/10.1002/2017GL075647>
- Su, C., Fan, D., Jiang, J., Sun, Z., Liu, Y., Song, W., Wan, Y., Yang, G., & Qiu, W. (2021). Self-Consistent Thermodynamic Parameters of Diopside at High Temperatures and High Pressures: Implications for the Adiabatic Geotherm of an Eclogitic Upper Mantle. *Minerals*, 11(12), 1322. <https://doi.org/10.3390/min11121322>
- Takei, Y. (1998). Constitutive mechanical relations of solid-liquid composites in terms of grain-boundary contiguity. *Journal of Geophysical Research: Solid Earth*, 103(B8), 18183–18203. <https://doi.org/10.1029/98JB01489>
- Timoshenko, S., & Goodier, J. N. (1969). *Theory of Elasticity*. McGraw-Hill. ISBN: 978-0-07-064270-6
- Tommasi, A., & Ishikawa, A. (2014). Microstructures, composition, and seismic properties of the Ontong Java Plateau mantle root. *Geochemistry, Geophysics, Geosystems*, 15(11), 4547–4569. <https://doi.org/10.1002/2014GC005452>
- Vauchez, A., Dineur, F., & Rudnick, R. (2005). Microstructure, texture and seismic anisotropy of the lithospheric mantle above a mantle plume: Insights from the Labait volcano xenoliths (Tanzania). *Earth and Planetary Science Letters*, 232(3-4), 295–314. <https://doi.org/10.1016/j.epsl.2005.01.024>
- Walker, A. M. (2012). The effect of pressure on the elastic properties and seismic anisotropy of diopside and jadeite from atomic scale simulation. *Physics of the Earth and Planetary Interiors*, 192-193, 81–89. <https://doi.org/10.1016/j.pepi.2011.10.002>